

A novel inversion algorithm for weak gravitational lensing using quasi-conformal geometry

Jan Jakob¹

Institute for Theoretical Astrophysics, Heidelberg University, Albert-Ueberle-Strasse 2, 69120 Heidelberg
e-mail: jan.jakob@campus.lmu.de

Preprint published in January 2025

ABSTRACT

Context. One of the challenges in weak gravitational lensing by galaxies and clusters is to infer the projected mass density distribution from gravitational lensing measurements, which is known as inversion problem.

Aims. We introduce a novel theoretical approach to solve the inversion problem. The cornerstone of the proposed method lies in a complex formalism that describes the lens mapping as quasi-conformal mapping with the Beltrami coefficient given by the negative of the reduced shear, which is, in principle, observable from the image ellipticities.

Methods. We propose an algorithm called QCLens that is based on this complex formalism. QCLens computes the underlying quasi-conformal mapping with a finite element approach by reducing the problem to two elliptic partial differential equations (PDEs) solely depending on the reduced shear field.

Results. Experimental results for both the Schwarzschild and singular isothermal lens demonstrate the agreement of our proposed method with the analytically computable solutions.

Key words. astrophysics: observations / techniques: quasi-conformal mappings / methods: elliptic PDE inversion / gravitational lensing: weak

1. Introduction

Gravitational lensing has become one of the most important fields in present-day astronomy, largely driven by considerable improvements in observational capabilities. Its distinguished feature of being independent of the nature and physical state of the deflecting mass makes it perfectly suited to study dark matter in the universe. In recent years, interest has increased in exploring the two most dominant components of the universe: dark matter and dark energy. To this end, large-scale imaging and spectroscopic surveys are currently in process, such as the *Euclid* mission (Euclid Collaboration: Y. Mellier and others (2024)), launched in July 2023, the *Rubin* Observatory Legacy Survey of Space and Time (Brough et al. (2020)), and the Roman Space Telescope (Spergel et al. (2015)) set to begin in late 2025, which will map the sky with unprecedented accuracy. A prominent cosmological probe for these surveys is weak gravitational lensing.

Weak gravitational lensing refers to the subtle distortions observed in the images of distant galaxies caused by the gravitational influence of massive structures along the line of sight. This phenomenon manifests in two primary ways: A convergence field κ leads to the magnification or demagnification of the background galaxies' images, altering their apparent size and brightness, while the shear γ stretches the galaxies' shapes, causing them to appear more elliptical or skewed than they intrinsically are.

The convergence field κ cannot be observed directly due to the mass-sheet degeneracy (Bartelmann & Schneider (2001); Kilbinger (2015)). Physically, it represents the projected total

matter density along the line of sight, modulated by a lensing kernel in the mid-distance between the observer and the galaxy sources. A widely used algorithm for mass mapping is the Kaiser-Squires method (Kaiser & Squires (1993)), which operates as a simple linear operator in Fourier space. However, this method has limitations, such as not accounting for missing data or the effect of noise.

In this paper, we propose to use a complex formalism for weak lensing, first introduced by Straumann (1997) to describe the lens mapping as quasi-conformal mapping with Beltrami coefficient field given by the negative of the reduced shear, which can be deduced from the observed image ellipticities. The resulting quasi-conformal mapping can then be broken down into two elliptical PDEs for each component of the complex deflection angle field. To our knowledge, this is the first time that solving quasi-conformal mappings is proposed for mass-map reconstruction.

This paper is structured as follows. In Sect. 2 we introduce the formalism of weak gravitational lensing and describe the mass-map reconstruction problem. Here, we also provide a brief overview of the current algorithm of Kaiser-Squires. Section 3 shows that weak lensing corresponds to a quasi-conformal mapping from the image to the source plane. We then present our proposed inversion method in Sect. 4. The method is novel in the sense that it exploits the property of the lens mapping to be quasi-conformal. Section 5 illustrates the feasibility of the proposed method by comparing the computed solutions with the analytical solutions for both the Schwarzschild and singular isothermal sphere lens model.

2. Weak-lensing mass mapping

Gravitational lensing occurs when light from distant galaxies bends around a foreground mass distribution. This phenomenon distorts the appearance of these galaxies, with the extent of distortion depending on the shape and size of the mass distribution along the line of sight. The relationship between the original source coordinates (β) and the observed, lensed image coordinates (θ) is described by the lens equation (e.g. Umetsu (2020))

$$\beta = \theta - \nabla\psi(\theta), \quad (1)$$

where ψ describes the lensing potential. By introducing local Cartesian coordinates $\theta = (\theta_1, \theta_2)$ centered on a certain reference point in the image plane, the Jacobian matrix of the lens mapping describing the local properties of lensing becomes

$$\mathcal{A}(\theta) := \frac{\partial\beta}{\partial\theta} = \begin{pmatrix} 1 - \psi_{11} & -\psi_{12} \\ -\psi_{12} & 1 - \psi_{22} \end{pmatrix}, \quad (2)$$

with $\psi_{i,j} = \partial^2\psi/\partial\theta_i\partial\theta_j$ ($i, j = 1, 2$). Alternatively, the components can be written as $\mathcal{A}_{ij} = \delta_{ij} - \psi_{ij}$, where δ_{ij} denotes the Kronecker delta. It is convenient to decompose \mathcal{A} by means of the Pauli matrices σ_a ($a = 1, 2, 3$) as

$$\mathcal{A} = (1 - \kappa)\mathcal{I} - \gamma_1\sigma_3 - \gamma_2\sigma_1. \quad (3)$$

κ is called *convergence* and defined as one half of the Laplacian of ψ :

$$\kappa := \frac{1}{2}(\psi_{11} + \psi_{22}) = \frac{1}{2}\Delta\psi, \quad (4)$$

with $\Delta = \nabla_{\theta}^2$. γ_1 and γ_2 are the two components of the *shear* γ , which can be considered as a complex quantity $\gamma(\theta) := \gamma_1(\theta) + i\gamma_2(\theta)$. κ , γ_1 and γ_2 are linear combinations of the second order derivatives of ψ :

$$\gamma_1 := \frac{1}{2}(\psi_{11} - \psi_{22}), \quad (5)$$

$$\gamma_2 := \frac{1}{2}(\psi_{12} + \psi_{21}) = \psi_{12}. \quad (6)$$

Equation (4) can be regarded as a two-dimensional Poisson equation,

$$\Delta\psi(\theta) = 2\kappa(\theta) \quad (7)$$

with inhomogeneity 2κ . Often one assumes that the field size is (hypothetical) infinite, i.e. it is sufficiently larger than the characteristic angular scale of the lensing cluster, but small enough for the flat-sky assumption to be valid. Then, the Green function becomes $\Delta^{-1}(\theta, \theta') = \ln|\theta, \theta'|/(2\pi)$, which yields ψ as convolution of Δ^{-1} with 2κ :

$$\psi(\theta) = \frac{1}{\pi} \int \ln(\theta - \theta')\kappa(\theta')d^2\theta'. \quad (8)$$

Using these new quantities, \mathcal{A} can be expressed as:

$$\mathcal{A}(\theta) = \begin{pmatrix} 1 - \kappa - \gamma_1 & -\gamma_2 \\ -\gamma_2 & 1 - \kappa + \gamma_1 \end{pmatrix}. \quad (9)$$

In the weak lensing limit ($|\kappa|, |\gamma| \ll 1$) we obtain

$$(\mathcal{A}^{-1})_{ij} \simeq (1 + \kappa)\delta_{ij} + \Gamma_{ij} \quad (i, j = 1, 2). \quad (10)$$

Γ_{ij} is the matrix defined by (Bartelmann and Schneider 2001; Crittenden et al. 2022):

$$\Gamma_{ij} = \left(\partial_i \partial_j - \delta_{ij} \frac{1}{2} \Delta \right) \psi(\theta). \quad (11)$$

Equation (9) illustrates that the convergence causes an isotropic change in the size of the source image, as it appears in the diagonal of the matrix \mathcal{A} . In contrast, the shear causes anisotropic distortions in the image shapes. The convergence κ can also be interpreted via equation (7) as a weighted projection of the mass density field between the observer and the source. By factoring out the term $(1 - \kappa)$ in Equation (9), the amplification matrix depends only on the reduced shear

$$\mathcal{A} = (1 - \kappa) \begin{bmatrix} 1 - g_1 & -g_2 \\ -g_2 & 1 + g_1 \end{bmatrix},$$

which is defined as

$$g := \frac{\gamma}{1 - \kappa}. \quad (12)$$

g can be directly measured in lensing surveys. For the subcritical regime where $\det\mathcal{A} > 0$ we can observe g directly, whereas for negative-parity regions with $\det\mathcal{A} < 0$ the quantity $1/g^*$ is observable.

In this paper we are interested in recovering the convergence κ from reduced shear data. This inverse problem is ill-posed due to the finite sampling of the reduced shear over a restricted survey area and the presence of shape noise in the measurements. However, in this work, the focus is not on addressing measurement limitations like done by Starck et al. (2021); instead, we present a theoretical approach that offers an alternative to the Kaiser-Squires method.

Kaiser-Squires. Following Meneghetti (2021), we give a short summary of the Kaiser-Squires inversion algorithm, which belongs to the class of free-form methods. In 1993, Kaiser and Squires developed an algorithm for reconstruction convergence maps from the observed weak lensing shear. This algorithm is today widely known as KS 93 algorithm. Since the shear and convergence are both linear combinations of the second-order derivatives of the lensing potential, they can be expressed in Fourier space as

$$\tilde{\kappa} = -\frac{1}{2}(k_1^2 + k_2^2) \tilde{\psi}, \quad (13)$$

$$\tilde{\gamma}_1 = -\frac{1}{2}(k_1^2 - k_2^2) \tilde{\psi}, \quad (14)$$

$$\tilde{\gamma}_2 = -k_1 k_2 \tilde{\psi}, \quad (15)$$

where $\tilde{\cdot}$ denotes the Fourier transform of the corresponding quantity and k_1, k_2 the elements of the wave vector k with norm square $k^2 = k_1^2 + k_2^2$. With the three independent equations, we can now eliminate $\tilde{\psi}$ and express γ as a function of κ :

$$\begin{pmatrix} \tilde{\gamma}_1 \\ \tilde{\gamma}_2 \end{pmatrix} = k^{-2} \begin{pmatrix} k_1^2 - k_2^2 \\ 2k_1 k_2 \end{pmatrix} \tilde{\kappa} = A \tilde{\kappa}, \quad (16)$$

with the operator

$$A := k^{-2} \begin{pmatrix} k_1^2 - k_2^2 \\ 2k_1 k_2 \end{pmatrix}. \quad (17)$$

A transforms the convergence to the shear vector in Fourier space. Using that A is idempotent ($AA^T = 0$), inverting equation (16) yields κ in dependence of γ :

$$\tilde{\kappa} = A^T \begin{pmatrix} \tilde{\gamma}_1 \\ \tilde{\gamma}_2 \end{pmatrix}. \quad (18)$$

We transform this relation back to real space by taking the inverse Fourier transform

$$\kappa(\theta) = \frac{1}{\pi} \int_{\mathbb{R}^2} [D_1(\theta - \theta')\gamma_1(\theta') + D_2(\theta - \theta')\gamma_2(\theta')] d^2\theta', \quad (19)$$

where D_1 and D_2 are appropriate kernel functions given by

$$D_1(\theta_1, \theta_2) = \frac{\theta_2^2 - \theta_1^2}{\theta^4}, \quad (20)$$

$$D_2(\theta_1, \theta_2) = \frac{2\theta_1\theta_2}{\theta^4}. \quad (21)$$

By defining the complex kernel function

$$D(\theta) = D_1(\theta) + iD_2(\theta), \quad (22)$$

equation (19) can be written as

$$\kappa(\theta) = \frac{1}{\pi} \int_{\mathbb{R}^2} \text{Re}[D^*(\theta - \theta')\gamma(\theta')] d^2\theta'. \quad (23)$$

As mentioned by [Seitz and Schneider 1996], under the assumption of vanishing shear at infinity, partial integration yields

$$\kappa(\theta) = \frac{1}{\pi} \int_{\mathbb{R}^2} \mathbf{H}^{KS}(\theta', \theta) \cdot \begin{pmatrix} \gamma_{1,1}(\theta') + \gamma_{2,2}(\theta') \\ \gamma_{2,1}(\theta') - \gamma_{1,2}(\theta') \end{pmatrix} d^2\theta', \quad (24)$$

with

$$\mathbf{H}^{KS}(\theta', \theta) = \frac{1}{2\pi} \frac{\theta - \theta'}{|\theta - \theta'|^2} = \nabla_{\theta'} \left(-\frac{1}{2\pi} \ln |\theta - \theta'| \right). \quad (25)$$

This means that in this limit the surface mass density is obtained by convolving the deflection angle field of a point mass with the first derivatives of the shear field.

3. Quasi-conformal mass mapping

Following Straumann (1997), we use the Wirtinger calculus to transform the basic lensing equations into a complex formulation. In particular, we will see that weak lensing corresponds to a quasi-conformal mapping from the image to the source plane with the Beltrami coefficient given by the reduced shear field g .

Wirtinger calculus. By identifying \mathbb{C} with \mathbb{R}^2 , we can write $z \in \mathbb{C}$ as $z = x + iy$ for $x, y \in \mathbb{R}$. Let U be an open subset of \mathbb{C} . The two 1-forms $dz = dx + idy$ and $d\bar{z} = dx - idy$ form a corresponding basis of the cotangent space of all points in U ($T_z U \cong \mathbb{C}$ for all $z \in U$). By defining the so called Wirtinger derivatives

$$\partial_z = \frac{\partial}{\partial z} := \frac{1}{2} \left(\frac{\partial}{\partial x} - i \frac{\partial}{\partial y} \right), \quad \partial_{\bar{z}} = \frac{\partial}{\partial \bar{z}} := \frac{1}{2} \left(\frac{\partial}{\partial x} + i \frac{\partial}{\partial y} \right), \quad (26)$$

we are able to represent the differential of any smooth complex function f on U as

$$df = \frac{\partial f}{\partial z} dz + \frac{\partial f}{\partial \bar{z}} d\bar{z}. \quad (27)$$

We introduce f_z and $f_{\bar{z}}$ for $\partial_z f$ and $\partial_{\bar{z}} f$, respectively, and denote with $\mathcal{D}(U)$ the \mathbb{C} -algebra of all functions $f : U \rightarrow \mathbb{C}$, which are infinitely often differentiable according to the real coordinates x and y . Then, according to the Cauchy-Riemann differential equations the vector space $\mathcal{O}(U)$ of holomorphic functions on U is equal to the kernel of the mapping $\partial_{\bar{z}} : \mathcal{D}(U) \rightarrow \mathcal{D}(U)$ (cf. Forster (2012)). With the Wirtinger derivatives the Laplacian can be expressed as

$$\Delta = 4\partial_z \partial_{\bar{z}}. \quad (28)$$

Differential of the lens mapping. By applying this formalism to the basic lens equation $\beta : \mathbb{R}^2 \mapsto \mathbb{R}^2, \theta \mapsto \beta(\theta)$ in (1), β can be written as complex function

$$f : \mathbb{C} \rightarrow \mathbb{C}, z \mapsto f(z) = z - 2\partial_{\bar{z}}\Psi = \partial_{\bar{z}}(z\bar{z} - 2\Psi). \quad (29)$$

Using (28) and (29) the Poisson equation (7) becomes

$$2\partial_z \partial_{\bar{z}} \Psi = \kappa, \quad (30)$$

and similar for the shear vector

$$\partial_{\bar{z}}^2 \Psi = \frac{1}{4}(\partial_1^2 - \partial_2^2)\Psi + \frac{i}{2}\partial_1 \partial_2 \Psi = \frac{1}{2}(\gamma_1 + i\gamma_2) = \frac{1}{2}\gamma. \quad (31)$$

With (29), (30) and (31) we can determine the differential of f :

$$df = \partial_z f dz + \partial_{\bar{z}} f d\bar{z} = (1 - \kappa)dz - 2\partial_{\bar{z}}^2 \Psi d\bar{z} = (1 - \kappa)dz - \gamma d\bar{z}. \quad (32)$$

Beltrami equation and quasi-conformal mappings. A function $f : \Omega_1 \rightarrow \Omega_2$, which is assumed to be at least continuously partial differentiable, between two domains Ω_1 and Ω_2 of the complex plane fulfills the *Beltrami equation*, if

$$f_{\bar{z}} = \mu f_z \quad (33)$$

holds on Ω_1 , where μ is a complex-valued function on Ω_1 and Lebesgue measurable. μ is called the *dilatation* or *Beltrami coefficient* of f and contains all information about the conformality of f . The Beltrami equation plays a crucial role in the theory of quasi-conformal mappings: f is said to be *quasi-conformal* (q.c.) if it fulfills the Beltrami equation (33) and

$$\|\mu\|_{\infty} = \text{esssup}_{x \in U} |\mu(x)| \leq k < 1 \quad (34)$$

holds for some $k \in \mathbb{R}$. Considering the Jacobian J_f of f given by

$$J_f = |f_z|^2 - |f_{\bar{z}}|^2 = |f_z|^2(1 - |\mu|^2). \quad (35)$$

It is clear that f is q.c. if it fulfills the Beltrami equation and preserves orientation ($J_f > 0$). Furthermore, $\mu \equiv 0$ if and only if f is conformal. Thus, q.c. mappings can be seen as generalizations of conformal mappings. Q.c. mappings are essential those homeomorphisms, which map infinitesimal circles to ellipses of bounded eccentricity (cf. Lui et al. (2013a)).

Lens equation as quasi-conformal mapping. By comparing (27) with (32), we obtain the Beltrami coefficient of the lens mapping as the negative of the reduced shear

$$\mu = \frac{f_{\bar{z}}}{f_z} = -\frac{\gamma}{1 - \kappa} = -g. \quad (36)$$

In the weak-lensing limit, where $\kappa, \gamma \ll 1$, the lens mapping does not only fulfill the Beltrami equation, but also $|g| \leq k < 1$ is satisfied for some $k \in \mathbb{R}$. Otherwise, the Jacobian J_f would become singular as in the case of multiple images and strong lensing. The lens equation f can therefore be interpreted as a

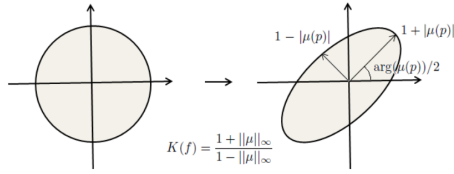


Fig. 1. Geometric interpretation of quasi-conformal mappings; Figure from Lui et al. (2013a)

quasi-conformal mapping, which is uniquely determined by the negative of the reduced shear as Beltrami coefficient and some appropriate boundary conditions.

As examples for lens mappings and their corresponding Beltrami coefficients, we consider the Schwarzschild and the singular isothermal lens two important examples of lenses. For the Schwarzschild lens we obtain

$$f(z) = z - \frac{1}{z}, \quad \mu = \frac{1}{z^2} \quad (37)$$

for the complex lens mapping and Beltrami coefficient, and for the singular isothermal lens

$$f(z) = z - \frac{z}{|z|}, \quad \mu = \frac{z^2}{2|z|^3 - |z|^2}. \quad (38)$$

In chapter 4 we compare the results of our proposed method against those analytically solvable examples to show the validity of our algorithm.

Geometric interpretation. We consider an infinitesimal ellipse field that is constructed in the following way: As shown in Figure 1, we assign each point $z \in U$ an infinitesimal circle that is mapped by f to an infinitesimal ellipse of bounded eccentricity

$$K_f(z) := \frac{|f_z| + |f_{\bar{z}}|}{|f_z| - |f_{\bar{z}}|} = \frac{1 + |\mu(z)|}{1 - |\mu(z)|}. \quad (39)$$

$K_f(z)$ is called *dilatation of f at z* . By taking the (essential) supremum over all points in U we obtain the notion of the *dilatation of f*

$$K_f := \operatorname{esssup}_{z \in U} K(f, z) = \frac{1 + \|\mu\|_\infty}{1 - \|\mu\|_\infty}, \quad (40)$$

which is well-defined for a q.c. mapping because of $1 - \|\mu\|_\infty \geq 1 - k > 0$. The argument of the major axis $a = 1 + |\mu(z)|$ of this infinitesimal ellipse can also be expressed in terms of the Beltrami coefficient by

$$\arg(1 + |\mu(z)|) = \arg(\mu(z))/2. \quad (41)$$

Geometrically this means that there is a fixed bound in the stretching for f in any given direction compared to any other direction. Solving the Beltrami equation (33) is then equivalent to find a function f whose associated ellipse field (with bounded eccentricity) coincides with the prescribed Beltrami coefficient field μ . This is just the inversion problem in gravitational lensing, where the negative of the reduced shear g takes over the role of μ .

4. Modelling with quasi-conformal mappings

4.1. Reduction to elliptic PDEs

The Beltrami equation (33) can be reduced to two elliptic PDEs for the real and imaginary part of f with coefficients determined by the Beltrami coefficient field μ (Lui et al. (2013b)). By decomposing μ and f into $\mu = \operatorname{Re}(\mu) + i\operatorname{Im}(\mu) =: \rho + i\tau$ and $f = \operatorname{Re}(f) + i\operatorname{Im}(f) =: u + iv$ the Beltrami coefficient can be written in terms of x and y derivatives of u and v as

$$\mu = \rho + i\tau = \frac{(v_x - v_y) + i(v_x + u_y)}{(u_x + v_y) + i(v_x - u_y)}. \quad (42)$$

v_x and v_y can be expressed as linear combinations of u_x and u_y

$$-v_x = \alpha_1 u_x + \alpha_2 u_y, \quad (43)$$

$$v_y = \alpha_2 u_x + \alpha_3 u_y, \quad (44)$$

with

$$\alpha_1 = \frac{(\rho - 1)^2 + \tau^2}{1 - \rho^2 - \tau^2}; \quad \alpha_2 = -\frac{2\tau}{1 - \rho^2 - \tau^2}; \quad \alpha_3 = \frac{(1 + \rho)^2 + \tau^2}{1 - \rho^2 - \tau^2}. \quad (45)$$

On the other hand

$$u_y = \alpha_1 v_x + \alpha_2 v_y, \quad (46)$$

$$-u_x = \alpha_2 v_x + \alpha_3 v_y. \quad (47)$$

Due to the symmetry of the second derivatives it holds

$$\nabla \cdot \begin{pmatrix} -v_y \\ v_x \end{pmatrix} = 0 \quad \text{and} \quad \nabla \cdot \begin{pmatrix} u_y \\ -u_x \end{pmatrix} = 0. \quad (48)$$

By substituting equation (43) and (44) into equation (48) we obtain two elliptic PDEs for u and v

$$\nabla \cdot \left(A \begin{pmatrix} u_x \\ u_y \end{pmatrix} \right) = 0 \quad \text{and} \quad \nabla \cdot \left(A \begin{pmatrix} v_x \\ v_y \end{pmatrix} \right) = 0, \quad (49)$$

where the symmetric, positive definite matrix A is given by

$$A = \begin{pmatrix} \alpha_1 & \alpha_2 \\ \alpha_2 & \alpha_3 \end{pmatrix}. \quad (50)$$

The eigenvalues λ_1 and λ_2 of A

$$\lambda_1 = (1 - |\mu|)^2, \quad (51)$$

$$\lambda_2 = (1 + |\mu|)^2, \quad (52)$$

are strictly greater than 0, since $|\mu| \leq k < 1$. Since a_{ij} , α_1 , α_2 and α_3 do not explicitly depend on x or y , equation (49) can be written out as

$$-\operatorname{div}(A \nabla u) = - \sum_{i=1}^2 \partial_i (A \nabla u)_i = - \sum_{i,k=1}^2 a_{ik} \partial_{ik} u. \quad (53)$$

With that we can define the two linear elliptic differential operators

$$Lu := - \sum_{i,k=1}^2 a_{ik} \partial_{i,k} u, \quad (54)$$

$$Lv := - \sum_{i,k=1}^2 a_{ik} \partial_{i,k} v. \quad (55)$$

The analytical characteristics of the two differential operators are governed by the properties of g , such as adherence to the maximum principle. Similarly, the regularity of g plays a critical role in determining the regularity of the associated lens mapping, particularly with respect to interior regularity. In this work, however, we focus on solving $Lu = 0$ and $Lv = 0$ numerically with appropriate boundary conditions.

4.2. QCLens algorithm

Algorithm 1 QCLens algorithm

Input: planar domain Ω ; map of the reduced shear g (in principle observable); boundary conditions for real and imaginary part of the lens mapping f (Dirichlet, Neumann or mixed)

Output: lens mapping f (or deflection field β); map of convergence κ and shear γ

- 1: $\mu(z) = -g(z) \quad \forall z \in \Omega$
- 2: Compute $\alpha_1 = \frac{(\rho-1)^2 + \tau^2}{1-\rho^2-\tau^2}$; $\alpha_2 = -\frac{2\tau}{1-\rho^2-\tau^2}$; $\alpha_3 = \frac{(1+\rho)^2 + \tau^2}{1-\rho^2-\tau^2} \quad \forall z \in \Omega$ where $\mu(z) = \rho(z) + i\tau(z)$
- 3: Define the positive definite matrices $A(z) := \begin{pmatrix} \alpha_1(z) & \alpha_2(z) \\ \alpha_2(z) & \alpha_3(z) \end{pmatrix} \quad \forall z \in \Omega$
- 4: **for** $w \in \{u = \text{Re}(f), v = \text{Im}(f)\}$ **do**
- 5: Solve the elliptic PDE $-\text{div}(A \nabla w) = 0$ on Ω
- 6: **end for**
- 7: $\kappa = \frac{1}{2}(u_x + v_y)$; $\gamma_1 = \frac{1}{2}(u_x - v_y)$ and $\gamma_2 = \frac{1}{2}u_y$

The implementation of the QCLens algorithm utilizes the HiFlow3 software (Heuveline (2010)), a C++-based multi-purpose finite element solver. This approach discretizes the problem by employing a triangulation of the domain Ω with mesh width h . The Beltrami coefficient $-g$ is used to calculate the matrices A at each node. These matrices are integrated over the mesh using a two-dimensional quadrature formula to form the stiffness matrix and right-hand side vector. For solving the resulting elliptic PDEs for both the real and imaginary parts of the lens mapping, finite element methods (FEM) are employed. Specifically, piecewise linear functions are used to represent the solution in a finite-dimensional subspace. The solution is computed iteratively using a conjugate gradient (CG) solver, with boundary conditions defined as Dirichlet or Neumann based on physical assumptions about the deflection field at the boundary $\partial\Omega$.

In the spirit of reproducible research, the QCLens algorithm is publicly available on GitHub¹, including the material needed to reproduce the simulated experience (folder weak lensing experiments/).

¹ <https://github.com/JanJakob1/weak-lensing>

4.3. Extension to the sphere

Inversion methods for large areas of the sky, where the plane sky approximation can not be longer be assumed, have become highly relevant with Stage IV surveys like Euclid (Euclid Collaboration: Y. Mellier and others (2024)). Imminent, extending mass-mapping techniques to the sphere is a fundamental necessity for such surveys. A traditional approach is to decompose the sphere into overlapping patches, assume a flat approximation on each individual patch, reconstruct each patch independently, and finally, recombine all patches on the sphere. It is natural to ask whether our results of the planar case can be generalized to the curved-sky treatment: If the plane sky approximation is considered as a coordinate chart around a given point on the curved surface, the Beltrami equation holds locally in this chart. Unfortunately, the flat sky approximation does not provide isothermal coordinate charts. To what extent the lens mapping can still be described in this setting as a quasi-conformal mapping between curved surfaces will be the subject of future work.

5. Experimental results

5.1. Schwarzschild Lens

For the Schwarzschild lens we obtain for the lens mapping

$$f(z) = z - \frac{1}{z} = x \left(1 - \frac{1}{x^2 + y^2} \right) + iy \left(1 - \frac{1}{x^2 + y^2} \right) \quad (56)$$

$$=: u(x, y) + iv(x, y),$$

and for the Beltrami coefficient

$$-\mu(z) = \frac{1}{\bar{z}^2} = \frac{x^2 - y^2}{(x^2 + y^2)^2} + i \frac{2xy}{(x^2 + y^2)^2} =: \rho(x, y) + i\tau(x, y). \quad (57)$$

For both the real and imaginary part of f , we assume Dirichlet boundary conditions. We compute u^n and v^n using the QCLens algorithm for different resolutions n from $n = 3$ to $n = 8$ (i.e. 2^n calls per coordinate direction). As shown in Figure 2, for $n = 7$ we obtain an almost complete agreement between the actual and calculated lens mapping.

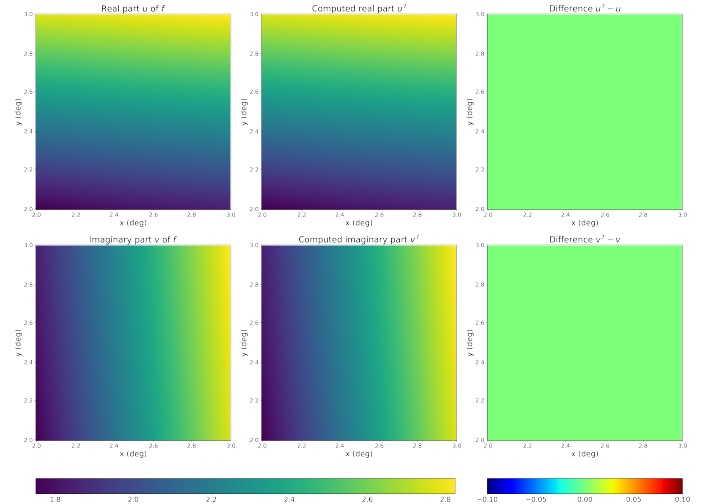


Fig. 2. Schwarzschild lens: Comparison between actual lens mapping $f = u + iv$ and calculated lens mapping $f^7 = u^7 + iv^7$ with QCLens for a resolution of $n = 7$ and Dirichlet boundary conditions.

Here, the coordinate system was chosen such that the point $(0, 0)$ coincides with the position of the point mass in the lens plane.

Additionally, the field of view Ω is assumed to be the square $\{z = x + iy \mid 2 \leq x, y \leq 3\}$, such that we are in the weak lensing regime and cross no critical curve. As shown in Figure 3, the deviation between the real and calculated lens mapping can also be quantified by plotting the L_2 and H_1 error against the refinement order n , where

$$e_{L_2,w}^n = \|w - w^n\|_{L_2} = \left(\int_{\Omega} (w(z) - w^n(z))^2 dz \right)^{\frac{1}{2}}, \quad (58)$$

$$e_{H_1,w}^n = \|\nabla(w - w^n)\|_{L_2} = \left(\int_{\Omega} |\nabla w(z) - \nabla w^n(z)|^2 dz \right)^{\frac{1}{2}}, \quad (59)$$

with $w \in \{u, v\}$. The errors $e_{L_2,w}^n$ and $e_{H_1,w}^n$ are the same for both u and v .



Fig. 3. Schwarzschild lens error: L_2 and H_1 errors for different refinement orders with Dirichlet boundary conditions. The orange and red lines overlap, as well as the green and blue line.

As can be seen in Figure 3, the error $e_{L_2,w}^n$ decreases quadratically with increasing refinement order n , while the error $e_{H_1,w}^n$ decreases linearly with n .

5.2. Singular Isothermal Lens

For the singular isothermal lens we obtain for the lens mapping

$$f(z) = z - \frac{z}{|\bar{z}|} = x \left(1 - \frac{1}{\sqrt{x^2 + y^2}} \right) + iy \left(1 - \frac{1}{\sqrt{x^2 + y^2}} \right) \quad (60)$$

$$=: u(x, y) + iv(x, y),$$

and for the Beltrami coefficient

$$\mu(z) = \frac{z^2}{2|\bar{z}|^3 - |\bar{z}|^2} = \frac{(x^2 - y^2)}{2(x^2 + y^2)^{\frac{3}{2}} - (x^2 + y^2)} + i \frac{2xy}{2(x^2 + y^2)^{\frac{3}{2}} - (x^2 + y^2)}$$

$$=: \rho(x, y) + i\tau(x, y). \quad (61)$$

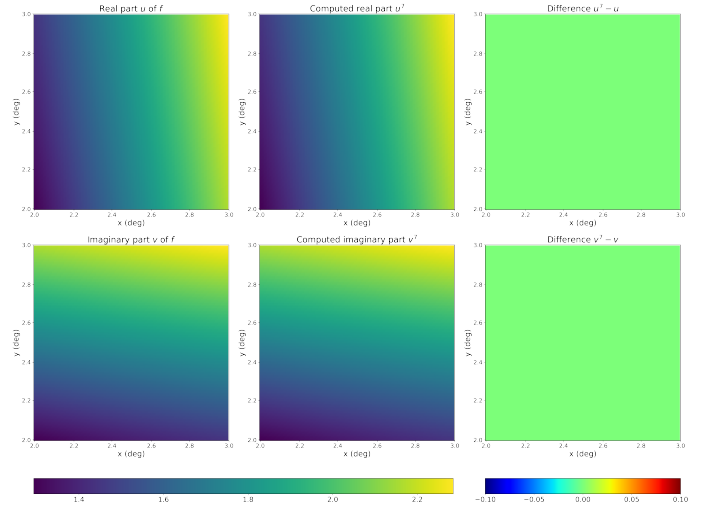


Fig. 4. Singular isothermal lens: Comparison between actual lens mapping $f = u + iv$ and calculated lens mapping $f^7 = u^7 + iv^7$ with QCLens for a resolution of $n = 7$ and Dirichlet boundary conditions.

Using the same coordinate system and field of view as for the Schwarzschild lens, we obtain similar results under the assumption of Dirichlet boundary conditions.



Fig. 5. Singular isothermal lens error: L_2 and H_1 errors for different refinement orders with Dirichlet boundary conditions. The orange and red lines overlap, as well as the green and blue line.

6. Conclusions

We proposed a novel inversion algorithm for weak gravitational lensing based on the quasi-conformal mapping framework. By reformulating the lens equation as a Beltrami equation, the problem was reduced to solving elliptic PDEs for the real and imaginary parts of the lens mapping. The QCLens algorithm was applied to analytically solvable cases, such as the Schwarzschild and singular isothermal lens models, demonstrating consistency with expected results. Additionally, we discussed the feasibility of extending the approach to spherical geometries, which will be necessary for future surveys like Euclid. These findings provide a foundation for further exploration of mass-mapping techniques within this framework.

Acknowledgements. We thank Prof. Björn Malte Schäfer for his early discussions on the subject and for valuable comments on earlier versions of the manuscript.

References

- Bartelmann, M. & Schneider, P. 2001, 340, 291
- Brough, S., Collins, C., Demarco, R., et al. 2020, arXiv preprint arXiv:2001.11067
- Euclid Collaboration: Y. Mellier and others. 2024, Astronomy & Astrophysics [arXiv:2405.13491]
- Forster, O. 2012, Lectures on Riemann Surfaces - (Berlin Heidelberg: Springer Science & Business Media)
- Heuveline, V. 2010, ACM Transactions on Mathematical Software, 37, 1
- Kaiser, N. & Squires, G. 1993, The Astrophysical Journal, 404, 441
- Kilbinger, M. 2015, Reports on Progress in Physics, 78, 086901
- Lui, L. M., Gu, X., & Yau, S.-T. 2013a, Convergence of an iterative algorithm for Teichmüller maps via generalized harmonic maps
- Lui, L. M., Lam, K. C., Wong, T. W., & Gu, X. 2013b, SIAM Journal on Imaging Sciences, 6, 1880
- Meneghetti, M. 2021, Introduction to Gravitational Lensing - With Python Examples (Singapore: Springer Nature)
- Spergel, D., Gehrels, N., Baltay, C., et al. 2015, Wide-Field InfraRed Survey Telescope-Astrophysics Focused Telescope Assets WFIRST-AFTA 2015 Report
- Starck, J.-L., Themelis, K. E., Jeffrey, N., Peel, A., & Lanusse, F. 2021, Astronomy & Astrophysics, 649, A30
- Straumann, N. 1997, Complex Formulation of Lensing Theory and Applications
- Umetsu, K. 2020, The Astronomy and Astrophysics Review, 28